Prediction-based Game-theoretic Strategy for Energy Management of Hybrid Electric Vehicles

Juanting Xu, Amro Alsabbagh, *Member, IEEE*, ChengbinMa, *Senior Member, IEEE*

***Abstract*—This paper studies a prediction-based energy management for onboard hybrid energy storage system (HESS), combining engine-generator (EG), battery, and ultracapacitor (UC). Each of these energy sources has a specific utility function to represent its unique preference. Thus, a game-theoretic strategy is presented to model the different preferences of these energy sources and their interactions, and hence to properly dispatch the power load demand among them. To further improve this power dispatch, i.e., the energy management, that may be influenced by the fluctuation of the uncertain power load demand, a prediction is included in the basic game-theoretic strategy to form a prediction-based game-theoretic strategy. The power load demand can be derived from the velocity in HESS and the velocity prediction is implemented by a long short-term memory (LSTM) network. An improvement on the accuracy of this prediction is achieved by utilizing feature extraction and time-series analysis. A multiple time-series method is newly applied to group the input features according to the target prediction horizon. The solution, i.e., Nash Equilibrium, of this proposed strategy is reached based on the best response functions of the energy sources and its performance is quantified by four criteria. Short-distance and long-distance driving in a broader scope are analyzed in simulation. Both the simulation and experiment results demonstrate the efficiency of the proposed strategy to smoothen the battery power with decreasing 0.01% in σ_{pb} (i.e., prolong battery life), to reduce the engine-generator power with reducing 0.01% in μ_{Eg} (i.e., deplete fossil fuels), and to lower the driving costs. Moreover, the robustness and sensitivity of the proposed strategy are validated through case studies with increasing velocity prediction error.**

***Index Terms*—Game theory, energy management, onboard hybrid energy storage system, long short-term memory, velocity prediction.**

NOMENCLATURE

U_g	Utility function of EG
U_b	Utility function of battery
U_c	Utility function of UC
U_{gc}	Utility function of the EG and UC combination
U_{bc}	Utility function of the battery and UC combination
P_g	EG Power
P_b	Battery power
P_c	UC power
P_l	Load power
P_g^*	Optimal EG power
P_{bave}	Average battery power
P_{blast}	Battery power in the last instant power
P_{bmax}	Maximum of battery power
P_{bmin}	Minimum of battery power
P_{bpre}	Average future battery power over horizon
P_{lpre}	Future load power
P_{cmax}	Maximum of UC power
P_{cmin}	Minimum of UC power
P_c^*	Optimal UC power
P_e	Engine power
ω_e	Rotational speed of engine
τ_e	Engine torque
V_{oc}	Open circuit voltage of battery model
V_{cini}	Initial voltage of UC
V_{cmax}	Maximum voltage of UC
V_{cmin}	Minimum voltage of UC
V_c	UC voltage
V_{bus}	Bus voltage
I_{cpre}	Future current of UC
C	Capacity of UC
Δt	Time step
λ	Ratio of battery power to load power
n_g	Normalization factor for EG power
n_b	Normalization factor for battery power
n_c	Normalization factor for UC power
h_o	Prediction horizon
h_i	Input horizon
Γ^t	Features for velocity prediction at time t
v^t	Velocity
a^t	Acceleration
c^t	Type of driving condition
i_t	Input gate of LSTM
f_t	Forget gate of LSTM
o_t	Output gate of LSTM
$\widetilde{C}_t$	Candidate cell status of LSTM
C_t	New cell status of LSTM
μ_{Eg}	Average engine power
μ_{pb}	Average battery power
σ_{pb}^2	Variance of battery power
μ_{Ec}	Average energy difference of UC
T	Total driving time

Manuscript received November 16, 2020; revised March 23, 2021 and May 13, 2021; accepted May 22, 2021. Date of current version June 1, 2021.
(Corresponding author: Amro Alsabbagh)

J. Xu graduated from the University of Michigan-Shanghai Jiao Tong University Joint Institute, Shanghai Jiao Tong University, Shanghai, China (e-mail: xujt17@alumni.sjtu.edu.cn).

A. Alsabbagh is a postdoctoral fellow at polytechnique Montreal, Quebec, Canada (e-mail: amro.alsabbagh@hotmail.com).

C. Ma is with the University of Michigan-Shanghai Jiao Tong University Joint Institute, Shanghai Jiao Tong University, Shanghai 200240, China (e-mail: chbma@sjtu.edu.cn).

I. INTRODUCTION

DUE to the increasing CO_2 emission and the depleting fossil fuels, electric vehicles have gained tremendous attention as considered to be environment-friendly vehicles in the field of transportation [1]. However, these electric vehicles are still facing several challenges for their widespread use.

Due to the limited power density of the electric vehicle's battery, a battery-ultracapacitor (UC) hybrid energy system was proposed to utilize the high power density of UC pack [2]. In addition, due to the limited energy capacity of the battery on the long-term, the battery-UC hybrid energy system could not serve for long-distance travels, and thus it would cause driving range anxiety [3]. Therefore, an onboard hybrid energy storage system (HESS), combining engine-generator (EG), battery, and UC pack, was introduced [4]. Since this onboard HESS has three energy sources with different characteristics, it is necessary to design an energy management strategy to properly and effectively distribute the power load of vehicle among them.

Several energy management strategies were proposed in the literature in this regard. Ref. [5] proposed a fuzzy logic-based energy management in a battery/UC hybrid energy system to control the state of charge (SOC) of UC and to smooth the battery power. A multi-agent distributed-based energy management in smart islands was proposed in Ref. [6] and the proposed distributed optimization was accomplished by using primal-dual method of multiplier. Ref. [7] applied a non-cooperative game theory-based strategy in the hybrid energy system that considered the behavior of each energy source. Energy management strategies such as the ideal average-constant-load demand-based control, the power-flow control and the game theory-based control had described and compared in Ref. [7] and concluded that the game theory-based approach had gained a better result. Ref. [8] proposed a game-theoretic strategy with a tuning process for the weight coefficients of the utility functions to further improve the flexibility of the energy management in real time. Although the above strategies showed good results, they did not consider the future information in the models. A machine learning based approach for energy management in renewable microgrids was proposed in Ref. [9] and it considered support vector machine to estimate the load demand. However, it only considered the coordinated charging scheme, only suitable for the centralized frameworks, and thus it was not possible to use it in a decentralized structure. A Stochastic management of hybrid AC/DC microgrid considering electric vehicles charging demands was investigated in Ref. [10] and a support vector machine was developed to model the uncertainty effects of the system. However, they mainly cared about the cost of power purchase and didn't consider the characteristics of components such as battery aging which is extremely important in HEV. A game-theoretic energy management with velocity prediction in hybrid electric vehicle was proposed in Ref. [11] and the characteristics of components were considered in performance criteria. But it didn't consider the power cost. Therefore, an distributed energy management with considering uncertainties, characteristics of components and power cost is importantly needed for onboard HESS. Due to the influences of the dynamic load demand fluctuations of the vehicle in the HESS, which mainly come from the dynamic driving velocities, a velocity prediction is needed to handle the uncertainties of the onboard HESS. It is expected that designing an energy management strategy with velocity (which as mentioned before can determine the load demand) prediction for the onboard HESS is importantly needed to prolong life of components and lower driving costs.

Several works in the literature were proposed to predict the vehicle velocity, which could be categorized into model-based prediction, big data-driven prediction and neural-network (NN) prediction. Ref. [12] used the model-based prediction (including the dynamic programming, deterministic model predictive control, equivalent consumption minimization strategy (ECMS) and optimal ECMS) and neural networks (including back propagation (BP-NN), layer recurrent (LR-NN) and radial basis function NN (RBF-NN)) to predict velocity and their performances were compared to concluded that the RBF-NN predictor got a better prediction precision and it is suitable for modeling comprehensive driving behaviors. Ref. [13] used a deep learning method based on big data including historical velocity, traffic conditions, road information and weather, to predict the future velocity profile. A two-level data-driven model on the basis of big data and neural network is proposed to predict future velocities [14]. Despite of the beauty of the aforementioned works, it is difficult to obtain a large amount of data from different resources and to analyze them in real time. Instead of relying on big data, Ref. [15] relied on historical velocities and a context-aware nonlinear autoregressive model with exogenous inputs to predict velocity. The velocity prediction was treated as a time series problem and solved by utilizing NN. Besides, unified multilayer perceptron and unified nonlinear autoregressive NN with external input NNs were compared in Ref. [16] for sequence prediction. Ref. [17] compared the multilayer perceptron and the long short-term memory (LSTM) network for estimation task and validated that the LSTM gained a better performance with being more sensitive to capture the peaks and valleys. A location-velocity-temporal attention LSTM model was proposed in Ref. [18] and the two temporal attention mechanisms were applied to the hidden state vectors from the location and velocity LSTM layers. In addition, LSTM network is appropriate to learn long-term dependency which is beneficial to learn sequence information [19], such as velocity profile. Standing on the shoulder of giants, the the LSTM network is selected for velocity prediction.

A. Motivation and Contribution

According to the above discussion of energy management strategies in the literature, an energy management strategy with velocity prediction is importantly needed to handle the uncertainties of the onboard HESS and lower driving costs with considering characteristics of components. It is interesting to note that there are different characteristics in the respective preference of each energy source in the HESS. For example, the EG is capable of providing long-term energy supply, thus its preference should be minimizing its fuel consumption as much as possible. The battery has higher energy density, but its cycle life is limited and will be largely affected by charging/discharging. Thus the preference of battery is to prolong its life. For UC, it is more "robust" and its preference is to maintain its capability of fast charging/discharging. To balance the different preferences, it is expected to take advantage of the characteristic of each component and represent interactions among them. It is well-known that game theory is a powerful mathematical tool to represent interactions among players who have different preferences. To the best knowledge of the authors, game theory is an effective distributed method to dispatch the power among multiple energy sources. Game theory has further applications to develop strategies with considering future information or uncertain conditions. It is expected that considering the predicted velocity information in the utility functions, i.e., preferences, of the different energy sources of onboard HESS will improve the performance of the energy management.

To this end, this paper proposes a game-theoretic energy management with velocity prediction to distribute vehicle power load in the onboard HESS among its energy sources. This strategy consists of two processes, namely velocity prediction and game theory-based power distribution. The velocity prediction is treated as a time-series problem and an LSTM network is implemented to predict future sequences. Compared with the previous work [11], feature extraction and multiple time-series method are further utilized to improve the accuracy of this velocity prediction. This predicted velocity information is added into the designed utility function for each component of the HESS and a prediction-based game-theoretic strategy is then implemented. The Nash Equilibrium of this strategy is reached based on the best response functions. Moreover, the performance is not only related to the characteristics of components such as battery, but also the power cost. Thus the driving cost analysis is implemented under the long-distance driving profile, which shows results in a broader scope, compared with the previous work in [11]. Below are the contributions of this paper:

1) Comparing with the existing game-theoretic energy management of the onboard HESS, a prediction-based game-theoretic energy management is proposed to handle the uncertainties mainly from the fluctuations of load demand. The predicted information is added into the utility functions of these energy sources, and then forms a non-cooperative game, which is for smoothing the fluctuations of the battery power, lowering the driving cost, and increasing the system efficiency.
2) Comparing with the conventional single time-series method, a multiple time-series method is newly applied to group the input features according to the target prediction horizon. In order to improve the velocity prediction accuracy, not only the time-series analysis, but also the feature extraction is implemented. More features such as acceleration and the type of driving condition are deeply extracted from velocity profile.

This paper is organized as follows. Section II describes the system configuration and modeling. Velocity prediction is implemented in Section III and the design of the game-theoretic energy management strategy of onboard HESS is presented in Section IV. A comparison analysis of the two game-theoretic strategies, i.e., with and without velocity prediction, in simulation and experiment is presented in Section V and Section VI, respectively. Finally, the conclusion is given in Section VII.

II. System Configuration and Modeling

The overall system configuration consists of two parts (i.e., stages), namely velocity prediction and power distribution, as shown in Fig. 1. For the prediction part, LSTM network is utilized to predict the velocity of the HESS. In the power distribution part, we focus on calculating the vehicle demanded power load and power consumption, on the basis of the aforementioned and predicted velocity and by utilizing the longitudinal vehicle dynamics model. This part also focuses on distributing the calculated demanded power load properly among the three existing energy sources in the HESS, i.e., EG, battery pack, and UC pack. The adopted topology of these three sources is a parallel-active topology, which can provide higher reliability and flexibility than other topologies [20]. As seen in this topology, the power from the EG and UC can be controlled by adjusting the duty cycles of their AC/DC and DC-DC converters while the battery is directly connected to the common bus, i.e., DC bus, to maintain the stability of its voltage.

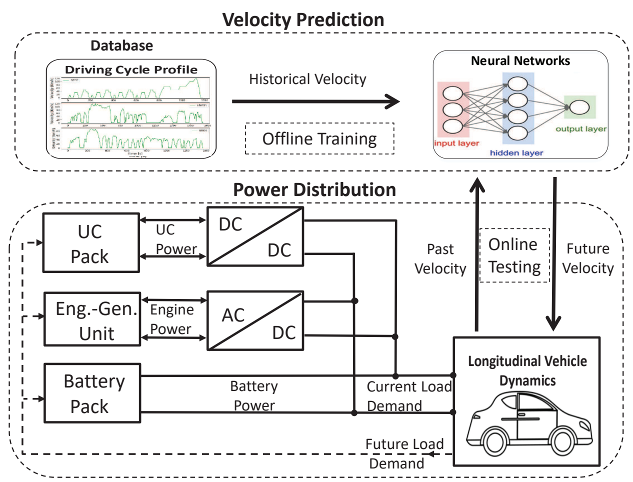

Fig. 1. System configuration.

In the HESS, the energy management problem is to dispatch power over the components i.e., EG, battery pack, and UC pack, with considering the performance of each component. Since there are different characteristic in the respective preference of each energy source in the HESS, they form a multi-objective problem with five criteria as shown in the simulation part. Take an example, the load demand from vehicle is $293.3W$, the EG, battery and UC pack decide their powers (i.e., $P_g = 30.2W, P_b = 36.7W$ and $P_c = 226.4W$) to match the requirement (i.e., $P_l = P_g + P_b + P_c$) and at the same time higher their own profits (i.e., the five criteria) as much as possible.

As shown in Fig. 1, the system consists of three energy sources (i.e., UC, battery, and engine-generator) and longitudinal vehicle dynamics. Here, we model each component.

1) Engine-generator: Similar to the model process in the [7], it is modeled based on the engine torque-speed map and generator efficiency map [7], as shown in Fig. 2. These two maps cooperatively determine the optimal power of engine at different power levels, as follows.

$$P_e = \tau_e \omega_e \tag{1}$$

$$P_g = \epsilon_{pc} \epsilon_g P_e \tag{2}$$

where the P_g is the final output power of the EG, P_e is the power of engine, ϵ_g is the efficiency of generator, ϵ_{pc} is the efficiency for conversing power, τ_e is the engine torque, and ω_e is the rotational speed of engine. For any P_g, there is only one corresponding optimal torque-speed couple.

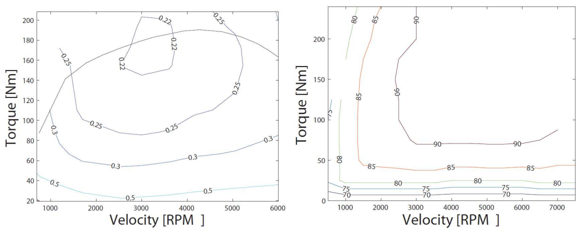

(a) (b)

Fig. 2. (a) Engine torque-speed map. (b)Generator efficiency map.

2) Battery pack: It is modeled by its equivalent circuit [7], as shown in Fig. 3(a). The equivalent circuit model of battery consists of open circuit voltage (V_{oc}), internal resistance (r_b), two resistance networks ($\tau_s = R_{t,s}, C_{t,s}$ and $\tau_t = R_{t,m}, C_{t,m}$). Through curve fitting experimental data, the V_{oc} and r_b are represented by two six-ordered polynomial functions as follows:

$$V_{oc} = w_{oc,0} + w_{oc,0}x + ... + w_{oc,6}x^6 \tag{3}$$

$$r_b = w_{r,0} + w_{r,1}x + ... + w_{r,6}x^6 \tag{4}$$

where x means the SOC of battery.

3) UC pack: It is also modeled by its equivalent circuit [7], as shown in Fig. 3(b). The equivalent circuit model of UC consists of capacitance (C), internal resistance ($R_{c,s}$) and leakage current modeling ($R_{c,p}$).

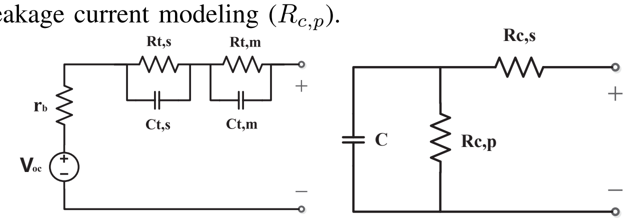

(a) (b)

Fig. 3. Equivalent circuit models of (a) Battery pack. (b) UC pack.

4) Longitudinal vehicle dynamics: This model is widely used to calculate the power demand for propelling the vehicle at a certain velocity, acceleration, and road condition [21]. This model is based on the free body of the vehicle, in which the applied forces on the vehicle are the aerodynamic force ($F_{aero} = -\rho C_d A v$), friction force ($F_{Tire} = \mu m g$), gravity force ($F_{grav} = mgsin\alpha$), and acceleration force ($F_{Traction} = m\alpha$), as shown in Fig. 4. The power consumption of a vehicle is calculated as $P_l = (F_A + F_R + F_U + F_{Accel})v$

III. VELOCITY PREDICTION

Predicting the velocity is a challenging issue, in which it is highly dynamic and hard to be explicitly represented by equations [12]. Thus, we utilize here a neural network

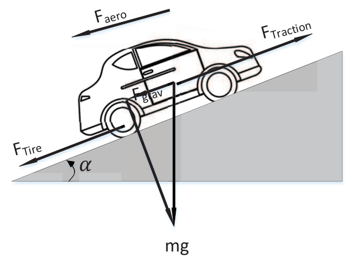

Fig. 4. Longitudinal vehicle dynamics model.

to predict the velocity because it can map an extremely nonlinear relationship between input and output [12]. Since it is difficult to obtain enough information, that is required for the velocity prediction, including historical driving data, weather information, traffic condition, and road information, we use here typical driving cycles as the dataset and we treat the prediction problem as a time-series problem [12]. Because the LSTM network can capture the long-term dependencies, it is suitable for time-series problem [19], and thus it is selected in this paper. Furthermore, to improve the accuracy of velocity prediction, a multiple time-series method is used to group the input features according to the target prediction horizon, comparing with the single time-series used in the above method. In addition, due to the limited dataset, feature extraction is applied to obtain the acceleration and the type of driving condition from the historical sequences, i.e., vehicle velocities of the typical driving cycles.

A. Dataset and Feature Extraction

As mentioned above, we use typical driving cycles, 18 driving cycles provided by the Driving Cycle Simulink Block in MATLAB here with time step of one second, to build the proper dataset, as shown in Fig. 5. These driving cycles are ARB02, CSHVR-Driver, CSHVR-Vehicle, NurembergR36, OCC, REP05, UDDSHDV, UNIF01, WVUCITY, WVUINTER, WVUSUB, Japanese JC08 Cycle, New European Driving Cycle (NEDC), INDIA-HWY-SAMPLE, optional air conditioning test SC03, aggressive driving US06, the air resources LA92, Urban Dynamometer Driving Schedule (UDDS). Out of these 18 driving cycles, NEDC and UDDS are selected as testing data whereas the others are used to train the adopted neural network model in this paper.

Each of these driving cycles has a certain velocity profile, i.e., value at each second during a specific period of time. Since this dataset has only one feature of velocity, it limits the prediction potential, accuracy, of the LSTM model. To overcome this issue, we obtain extra features from this dataset profile to characterize the operating dynamic state of the vehicle, such as acceleration and types of driving conditions. Thus the overall features for velocity prediction are velocity, acceleration and types of driving condition. To obtain the type of driving condition for each segment, we do the followings. The dataset in Fig. 5 is divided into segments with a time period of 60 seconds. Therefore, we can get the average velocity and average acceleration for each segment correspondingly. Based on the velocity profile, the acceleration/deceleration profile can be generated. Furthermore, the acceleration velocity ratio and uniform velocity ratio can also then be extracted.

Therefore, each segment can have four features, i.e., characteristics, namely the average velocity, average acceleration, acceleration velocity ratio, and uniform velocity ratio, which are further used to cluster the type of driving condition for each segment.

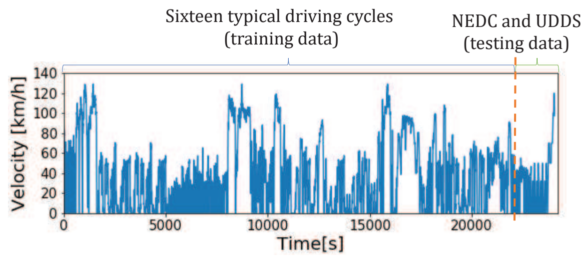

Fig. 5. The example dataset of velocity profile of 18 typical driving cycles.

We further cluster the types of driving conditions based on the average velocity, average acceleration, acceleration velocity ratio, and uniform velocity ratio. To do so, the k-means method is selected here to divide the driving condition into several types, as explained in the below steps:

1) Randomly choose K objects from N objects as the initial clustering centers.
2) Calculate the distance between each object and these center objects, and then reallocate these objects based on the minimum distance.
3) Recalculate the mean value of each cluster.
4) Calculate the distances between center objects and their former center objects. When it is within the error limitation, we keep the center objects unchanged and draw the conclusion that the function converges, so the algorithm terminates. If the conditions are not satisfied, return to step 2.

Note that for a better representation of the road conditions in real world, we classify here the driving conditions into four types, namely freeway, national highway, urban road, and low speed road, such as roads in campuses [11]The four types of driving conditions are digitalized as one, two, three, four to respectively represent the freeway, national highway, urban road, and low speed road.

B. LSTM Network

As mentioned before, the LSTM network is selected to predict the future velocity of the vehicle. To train this model, we utilize the aforementioned dataset. Here, the structure of the proposed LSTM network is shown in Fig. 6 (a) which has three layers, namely input, output, and one hidden layer in between. For a better visualization and representation, the LSTM cell in Fig. 6 (b) shows a zoomed-out version of the LSTM block. The LSTM cell as shown in Fig. 6 (b) has three gates, i.e., input gate i_t, forget gate f_t and output gate o_t. The d_t is the hidden state of the LSTM cell, which transfers message to the next cell. The $\widetilde{C}_t$ and C_t are candidate cell status and new cell status respectively.

$$i_t = \sigma(W_i[d_{t-1}, x_t] + b_i) \tag{5}$$
$$f_t = \sigma(W_f[d_{t-1}, x_t] + b_f) \tag{6}$$
$$o_t = \sigma(W_o[d_{t-1}, x_t] + b_o) \tag{7}$$

$$\widetilde{C}_t = tanh(W_c[d_{t-1}, x_t] + b_c) \tag{8}$$
$$C_t = i_t * \widetilde{C}_t + f_t * C_{t-1} \tag{9}$$
$$d_t = o_t * tanh(C_t) \tag{10}$$

The proposed LSTM network has one hidden layer with 30 neuron cells, while the number of the neurons in the input and output layer are determined by the dimensions of the input horizon h_i and the prediction horizon h_o, respectively. Note that the input of LSTM is a historical sequence of the features that explained in the previous section and the output is the future velocity sequence and the nonlinear relationship between them f_{NN} can be expressed as:

$$[v^{t+1}, \ldots, v^{t+h_o}] = f_{NN}(\mathit{\Gamma}^{t-h_i+1}, \ldots, \mathit{\Gamma}^{t}). \tag{11}$$

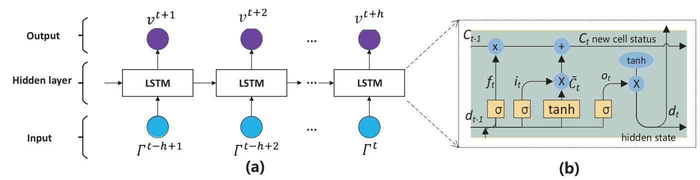

Fig. 6. (a) LSTM Network. (b) LSTM cell (zoomed-out version of LSTM block).

Basically, $\mathit{\Gamma}^t$ equals to the velocity v^t at time t. However, after the feature extraction that we proposed, it can be written that $\mathit{\Gamma}^t = [v^t, a^t, c^t]$, where v^t, a^t, c^t are the velocity, acceleration, and type of driving condition at time t, respectively. As explained earlier, here the time series analysis is performed on the input features through both single and multiple time-series methods to improve the prediction accuracy and are explained as in the follows.

1) Single time-series method: The prediction problem is regarded as a single time-series problem. The input-output pattern is shown in Fig. 7(a). Since there are 30 neurons in the hidden layer and each input passes through LSTM, the h_i inputs in this method go through $30 * h_i$ cells.

2) Multiple time-series method: We treat the prediction problem as a multiple time-series problem. The input features here are divided into several groups according to the target prediction horizon h_o, as shown in (12). Each group of input features corresponds to one output instant, as shown in Fig. 7(b). Each group has $\frac{h_i}{h_o}$ input instants and goes through $30 * \frac{h_i}{h_o}$ cells. The fraction of $\frac{h_i}{h_o}$ should be a positive integer because it represents the number of input instants, which is determined in this paper to be $\frac{h_i}{h_o} = 5$, i.e., $h_i = 5h_o$, based on simulation analysis in section V-A.

$$Inputs = \begin{cases} [\mathit{\Gamma}^{t-h_i+1}, \ldots, \mathit{\Gamma}^{t-h_i+(N-1)h_o+1}], \\ [\mathit{\Gamma}^{t-h_i+2}, \ldots, \mathit{\Gamma}^{t-h_i+(N-1)h_o+2}], \\ \ldots \\ [\mathit{\Gamma}^{t-h_i+h_o}, \ldots, \mathit{\Gamma}^{t}]. \end{cases} \tag{12}$$

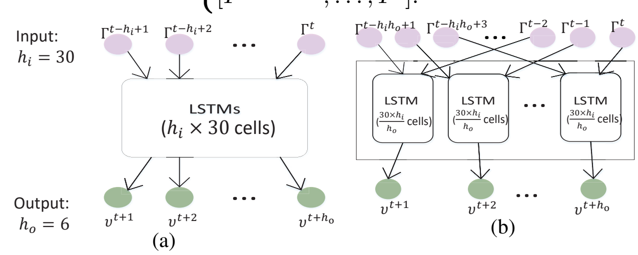

Fig. 7. (a) Single time-series method. (b) Multiple time-series method.

C. Comparison between the Two Time-series Methods

We compare here the performance in predicting the velocity between the single time-series method and the multiple time-series method. As mentioned in section III-A, the driving cycle NEDC and UDDS are chosen as the testing cycles. Furthermore, the comparison is conducted with three standard evaluation criteria of Mean Absolute Error (MAE), Mean Absolute Percentage Error (MAPE), and Root Mean Square Error (RMSE) [22].

As seen in Fig. 8 and Table I, the multiple time-series method can guarantee smaller errors in the selected criteria in the testing driving cycles NEDC and UDDS. Therefore, this method has a better performance, i.e., more accurate predicted velocities. Thus, we choose it for predicting the velocity prediction in this paper, as seen in the example two driving cycles NEDC and UDDS in Fig. 9.

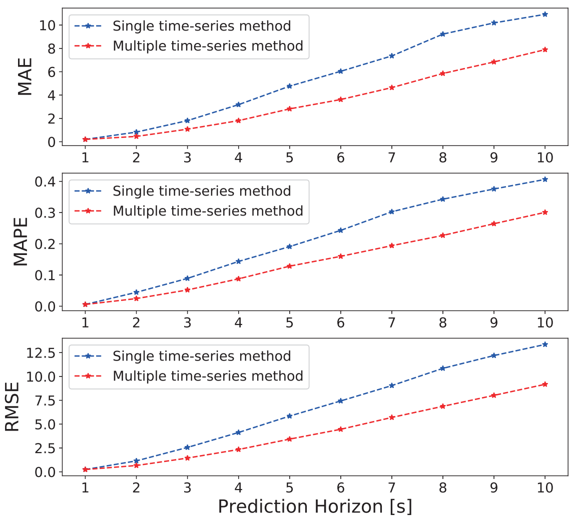

Fig. 8. Comparison in the velocity prediction performance between the two time-series methods.

TABLE I
COMPARISON BETWEEN THE TWO TIME-SERIES METHODS

Driving Cycle	Method	Evaluation Criterion		
		MAE	*MAPE*	*RMSE*
NEDC	Single time-series	6.144	0.241	7.428
	Multiple time-series	2.808	0.118	3.404
UDDS	Single time-series	7.610	0.564	10.283
	Multiple time-series	3.541	0.237	4.849

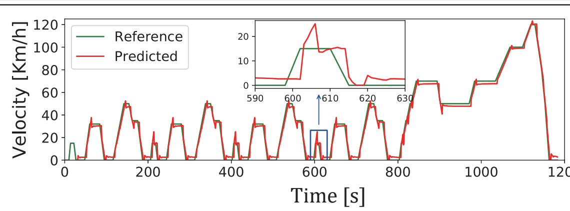

(a)

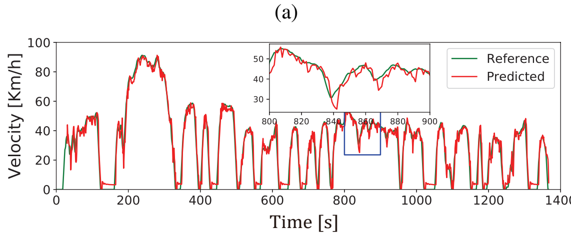

(b)

Fig. 9. The predicted velocity by the multiple time-series method in the two testing driving cycles (a) NEDC. (b) UDDS.

IV. POWER DISTRIBUTION

For the HESS with multiple sources, they naturally need a decentralized control strategy to distribute power (i.e., energy management). It is well-known that game theory is a powerful mathematical tool to represent interactions among players who have different preferences [7]. In this HESS, there are three players with different references and game theory can work fine to handle this application. To distribute the power in the onboard HESS among the three energy resources, i.e., EG, battery, and UC pack, game theory is properly utilized. In addition, there exist the uncertainties from the fluctuations of load demand in the onboard HESS, thus game-theoretic strategy with considering the uncertainties is importantly needed. To handle the uncertainties, the predicted velocity is combined to form the utility functions of these three energy sources. Base on the discussion above, we propose here a game-theoretic strategy with velocity prediction (GT-VP) which is compared with a game-theoretic strategy without velocity prediction (GT-NVP). To this end, a non-cooperative game is formulated, i.e., $G = [3, (P_g, P_b, P_c), (U_g, U_b, U_c)]$, in which the three energy sources of EG, battery, and UC pack are treated as selfish players with strategies of (P_g, P_b, P_c) and utility functions of (U_g, U_b, U_c) , respectively. At each control instant, each player determines its strategy, i.e., power, to maximize its own utility function. Furthermore, the solution of this game-theoretic strategy, i.e., Nash Equilibrium, is reached through the best response functions of the players.

A. Utility Functions

1) Engine-generator: Its preference is defined to maximize its fuel economy, and thus it is defined as in (13) to provide its power P_g as close as possible to its economical and optimal power P_g^* [8].

$$U_g = 1 - n_g(P_g - P_g^*)^2, \tag{13}$$

where n_g is a normalization factor [0,1]. In order to make the range of $n_g(P_g - P_g^*)^2$ between 0 to 1, it is defined as $n_g = \frac{1}{(P_g^*)^2}$.

It should be noted that since the optimal power P_g^* is a fixed value for each onboard HESS that depends on the characteristics of its engine-generator [7], the above utility function in both game-theoretic strategies (GT-VP and GT-NVP) are the same.

2) Battery pack: Its preference is defined to prolong its cycle life by the try to decrease the variation and magnitude of its power P_b [23]. To this end, the two-objective function (14) is designed. The w_{b1} and w_{b2} are the weight coefficients of the two sub-utility functions U_{b1} and U_{b2} for minimizing the power amplitude and power variation, respectively.

$$U_b = w_{b1}U_{b1} + w_{b2}U_{b2}, \tag{14}$$

$$U_{b1} = 1 - n_{b1}(P_b - P_{bave})^2, \tag{15}$$

$$U_{b2} = 1 - n_{b2}(P_b - P_{blast})^2. \tag{16}$$

where n_{b1} and n_{b2} are also normalization factors respectively defined by (17) and (18).

$$n_{b1} = min\left\{\frac{1}{(P_{bmax} - P_{bave})^2}, \frac{1}{(P_{bmin} - P_{bave})^2}\right\}, \tag{17}$$

$$n_{b2} = min\left\{\frac{1}{(P_{bmax} - P_{blast})^2}, \frac{1}{(P_{bmin} - P_{blast})^2}\right\}. \tag{18}$$

It should be noted that for the strategy (GT-NVP), the P_{bave} represents the average value of P_b within a period of time T from the beginning of driving cycle to the current control instant t, while in strategy (GT-VP) the period is extended to include the prediction horizon h_o by adding the average value of future battery power over this horizon P_{bpre}, which is determined by the predicted velocity, as designed in (19).

The λ in (21) is the ratio of battery power to load power P_l which is calculated from the historical power of battery and load.

$$P_{bave} = \begin{cases} \frac{1}{T}\sum_{i=1}^{T} P_b(i), & GT-NVP, \\ \frac{\sum_{i=1}^{T} P_b(i)+h_o P_{bpre}}{T+h_o}, & GT-VP, \end{cases} \tag{19}$$

$$P_{bpre} = \lambda \frac{\sum_{i=t+1}^{t+h_o} P_{lpre}(i)}{h_o}, \tag{20}$$

$$\lambda = \frac{1}{h_o}\sum_{i=t-h_o}^{t} \frac{P_b(i)}{P_l(i)}, \tag{21}$$

3) UC pack: Its preference is defined to maintain its energy capability for prolonging UC aging by making its power P_c , i.e., stored energy, as close as possible to its desired power P_c^* as in (22) after considering that n_c is a corresponding normalization factor [0,1].

$$U_c = 1 - n_c(P_c - P_c^*)^2, \tag{22}$$

$$V_{cini} = \sqrt{\frac{V_{cmax}^2 + V_{cmin}^2}{2}}, \tag{23}$$

$$P_c^* = 2P_{cmax} \cdot \left(\frac{V_c^2 - V_{cini}^2}{V_{cmax}^2 - V_{cini}^2}\right) - P_{cmax}. \tag{24}$$

where V_{cini} is the initial voltage of UC pack, V_{cmax} and V_{cmin} are the upper and lower bounds of the UC pack voltage, P_{cmax} is the maximum power of the UC pack, and V_c is the UC voltage. It should be noted here that V_c in the strategy (GT-NVP) represents the UC voltage at the current control instant t, while its value in the strategy (GT-VP) includes the future power load of the vehicle P_{lpre} that is obtained by its dynamics model with future velocity as in (25). Here, I_{cpre} is future current of UC pack, C is the capacity of the UC pack, Δt is the time step, P_l is power load of the vehicle, and V_{bus} is the bus voltage.

$$V_c = \begin{cases} V_{c,t}, & GT-NVP, \\ V_{c,t} - \frac{I_{cpre}\Delta t}{C}, & GT-VP, \end{cases} \tag{25}$$

$$I_{cpre} = \frac{P_{lpre} - P_l}{V_{bus}}. \tag{26}$$

B. Reduced Game and Nash Equilibrium

It is worth to note that under the energy conservation law the power of all units in the HESS that shown in Fig. 1 have to meet the following power constraint:

$$P_c = P_l - P_g - P_b. \tag{27}$$

Given (27), one player out of the three proposed players in the game-theoretic strategy can be represented by the left two players. In other words, if the UC pack is substituted by the other two players, the formulated game-theoretic strategy of the three players $G = [3,(P_g,P_b,P_c),(U_g,U_b,U_c)]$ can be reformulated into two-players game $G = [2,(P_{gc},P_{bc}),(U_{gc},U_{bc})]$. This is reasonable since the UC pack works as an energy buffer in the system. Thus, the utility function of the UC pack can be embedded into the utility functions of the other two players with proper weights. Therefore, the modified utility functions of the engine-generator U_{gc} and battery U_{bc} can be written as in (28) and (29), respectively. The weights in each equation (as eq. (31) and (32)) are summed to be one and the value of each weight is between zero to one as shown in eq. (30). Note that the weights here can be determined by several methods, such as the one in [7].

$$U_{gc} = w_g U_g + w_{cg} U_c, \tag{28}$$

$$U_{bc} = w_{b1}U_{b1} + w_{b2}U_{b2} + w_{cb}U_c. \tag{29}$$

$$0 < w_g, w_{cg}, w_{b1}, w_{b2}, w_{cb} < 1, \tag{30}$$

$$w_{b1} + w_{b2} + w_{cb} = 1, \tag{31}$$

$$w_g + w_{cg} = 1. \tag{32}$$

The solution, i.e., Nash Equilibrium, of the formulated game-theoretic strategy can be reached by the best response functions of the players [7]. The target best response functions can be obtained through the partial derivatives of the modified utility functions, i.e., $\frac{\partial U_{gc}}{\partial P_g} = 0$ and $\frac{\partial U_{bc}}{\partial P_b} = 0$. For the engine-generator, in order to maximize its own utility function U_{gc} , its decision P_g is solved using its own best response function in (33).

$$-2n_g w_g(P_g - P_g^*) + 2n_c w_{cg}(P_c - P_c^*) = 0, \tag{33}$$

For the battery, in order to maximize its own utility function U_{bc} , its decision P_b is solved using its own best response function in (34).

$$-2n_{b1}w_{b1}(P_b - P_{bave}) - 2n_{b2}w_{b2}(P_b - P_{blast}) + 2n_c w_{cb}(P_c - P_c^*) = 0. \tag{34}$$

As shown in Fig. 10, the convergence of P_g and P_b is iteratively achieved, namely the Nash Equilibrium of the Non-cooperative game, which proves the existence and uniqueness of Nash Equilibrium. The Nash Equilibrium is achieved with selected strategy and no player can benefit by changing strategy while the other players keep theirs unchanged [7].

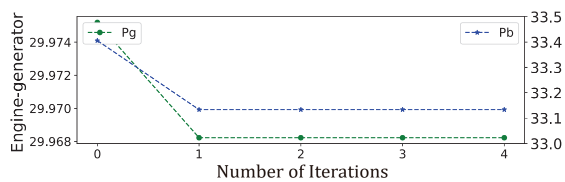

Fig. 10. Convergence to Nash Equilibrium at an example stage in the following simulation.

Consequently, the existence of Nash Equilibrium can be proved and the power dispatch in the HESS can be written as in (35) and (36). Note that since P_l is a known value, P_c can be then calculated by (27).

$$P_g = \frac{2n_g w_g P_g^* + 2n_c w_{cg}(P_l - P_b - P_c^*)}{2n_g w_g + 2n_c w_{cg}}, \tag{35}$$

$$P_b = \frac{2n_{b1}w_{b1}P_{bave} + 2n_{b2}w_{b2}P_{blast} + 2n_c w_{cb}(P_l - P_g - P_c^*)}{2n_{b1}w_{b1} + 2n_{b2}w_{b2} + 2n_c w_{cb}}. \tag{36}$$

V. Simulation Analysis

The simulation was implemented in real time under Python environment and the control instant for energy management is one second. The simulation includes two procedures, i.e., velocity prediction and energy management. The real-time velocity prediction of single time series for each step costs 0.359 milliseconds and that of multiple time series costs 1.039 milliseconds. Although the multiple time series method gives higher computational burden, it can give the prediction within the instant control time step (i.e., one second) of the proposed game theory. Therefore the computational burden can still be implemented in real-time for this application of HESS. Here the simulation analysis is divided into two parts. The first part is dedicated to determine the prediction horizon of velocity h_o. While the second is conducted to compare the performance of the two game-theoretic strategies, i.e., GT-NVP and GT-VP. Following the evaluation criteria of the multi-objective problem in the literature, four criteria are introduced to measure the performance within the three players in the HESS as shown in (37)-(40) as well as the overall performance of all the players as expressed in (41).

$$\mu_{Eg} = \frac{1}{T}\sum_{i=1}^{T} P_g(i), \tag{37}$$

$$\mu_{pb} = \frac{1}{T}\sum_{i=1}^{T} P_b(i), \tag{38}$$

$$\sigma_{pb}^2 = \frac{1}{T}\sum_{i=1}^{T} (P_b(i) - \mu_{pb})^2, \tag{39}$$

$$\mu_{Ec} = \frac{1}{T}\sum_{i=1}^{T} \left| \frac{1}{2}Cv_c^2(i) - \frac{1}{2}CV_{cini}^2 \right|, \tag{40}$$

$$\rho = \sqrt{N(\mu_{Eg})^2 + (1 - N(\mu_{pb}))^2 + N(\sigma_{pb})^2 + N(\mu_{Ec})^2}, \tag{41}$$

$$N(x) = \frac{x - x_{min}}{x_{max} - x_{min}}, \tag{42}$$

where μ_{Eg} is the average engine power, μ_{pb} is the average battery power, σ_{pb}^2 is the variance of battery power, μ_{Ec} is the average energy difference between the energy stored in the UC pack and the desired initial energy, T is the total driving time, i is the present driving time, and $N(\cdot)$ is a normalization function of the argument x between its minimum value x_{min} and its maximum value x_{max}. The less energy supplied by engine-generator μ_{Eg} means saving more fossil fuels, the more average battery power μ_{pb} and less variance of battery power σ_{pb}^2 reflect to extend battery aging, and the less average UC energy difference μ_{Ec} means prolonging UC aging. Therefore, it should be noted that it is preferred to have less energy supplied by engine-generator μ_{Eg}, more average battery power μ_{pb}, less variance of battery power σ_{pb}^2, and less average UC energy difference μ_{Ec}. Thus, it is obvious that a lower value of overall performance ρ indicates better performance.

A. Determination of Prediction Horizon of Velocity

Since the performance of the power dispatch is the aim of this paper, the determination of the prediction horizon for velocity is designed on the overall performance of the proposed GT-VP strategy. The the prediction horizon h_o is changed between 1 to 10 with offline simulation analysis on the historical driving profiles and the overall performance ρ is tracked in Fig. 11. It is clear to conclude that the best performance, i.e., the lowest value of ρ, can be reached when the prediction horizon $h_o = 6$, and thus its value is set as 6.

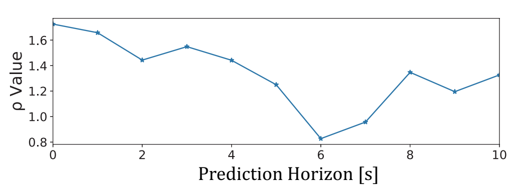

Fig. 11. Overall performance at different prediction horizons of velocity.

B. Comparison Between the Two Game-theoretic Strategies

As mentioned before, the two driving cycles NEDC and UDDS are selected as the testing data for the comparison between the two game-theoretic energy management strategies, in which two cases are studied.

1) Short-distance driving: Fig. 12 shows the power dispatch among the three players in a single run of the testing driving cycle NEDC, in which the green curves indicate to the results form the GT-NVP whereas the red curves refer to the results from the GT-VP. The contributed power from each player follows its preference that is designed by its objective function. It is obvious that the results of both strategies follow the same general trend. However, there is a difference between the results, and thus some enlarged segments are illustrated. In addition, Table II is introduced for further detailed comparison. As it can be seen from μ_{Eg}, the power of engine-generator in GT-VP is decreased by 0.010 % compared with that in GT-NVP. This means less use in oil, i.e., saving money and cleaner environment. This results from the reason that the average battery power μ_{pb} of GT-VP is larger than that of GT-NVP, i.e., increase by 12.06%, which means again that more clean energy is used in GT-VP. The variation of the battery power σ_{pb} in GT-VP is smaller, i.e., smoother, by 1.12% than that in GT-NVP. As described in section IV-A, decreasing the variation of battery power is effective to prolong the battery life, and thus the GT-VP strategy is more successful than GT-NVP in this reagrd. Finally, although the average energy difference of UC pack in GT-VP is increased by 0.107%, it does not matter because the UC pack works as an energy buffer and it has a high power density. Similar to NEDC, the quantified performance of the UDDS driving cycle in the Table II also demonstrates that the proposed GT-VP is more effective than the GT-NVP.

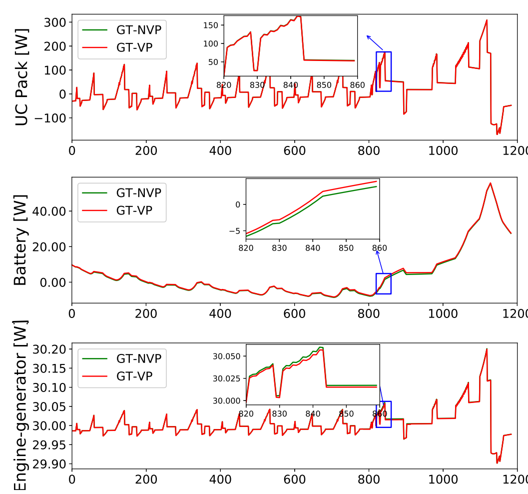

Fig. 12. Power dispatch among the players in the NEDC driving cycle.

TABLE II
THE COMPARISON OF EVALUATION CRITERIA IN SIMULATION

Driving Cycle	**Index**	**Evaluation Criterion** $\mu_{Eg}(w)$	$\mu_{pb}(w)$	$\sigma_{pb}(w^2)$	μ_{Ec}(J)
NEDC	GT-NVP	30.046	3.605	182.176	30785
	GT-VP	30.043	4.040	180.146	30818
	Percentage	-0.010%	12.06%	-1.12%	0.107%
UDDS	GT-NVP	29.994	12.570	55.496	30065
	GT-VP	29.992	12.619	54.659	30079
	Percentage	-0.007%	0.390%	-1.51%	0.047%

Due to the unavoidable error and noise in the velocity prediction, the analysis of robust and sensitivity of the proposed prediction-based strategy is necessary. We study the robustness and sensitivity issue of the proposed approach

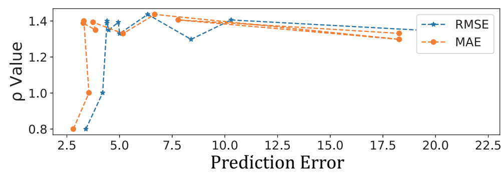

Fig. 13. Overall performance at different prediction error of velocity.

through case studies with increasing velocity prediction error. To generate the case studies, velocity prediction with fewer layers, fewer training steps and fewer neural cells is carried out to increase the prediction error. Then the prediction-based game-theoretic strategy is implemented to calculate evaluation criteria and overall performance (i.e., ρ value, lower ρ means better performance) for each case. From Fig. 13, we can see that the ρ value is increased and then keeps stable when the prediction error increases gradually. Although the overall performance becomes gradually worse when the prediction error becomes larger, it finally keeps at the same level. Besides, the overall performance will change even though the prediction error slightly change. Therefore, the robustness and sensitivity of the proposed prediction-based strategy are validated.

2) Long-distance driving: In order to compare the two game-theoretic strategies from a broader scope, the NEDC driving cycle is repeated sixteen times with different initializations to form a long-distance driving profile. The overall performance ρ of the two game-theoretic strategies in this designed driving profile is shown in Fig. 14, in which two observations can be seen. The first is that the ρ value of GT-VP is always lower than that of GT-NVP. It is worthy to mention, as described in section V-A, that a lower value of ρ means a better performance. The second point is that the difference in the value of ρ between the two game-theoretic strategies is gradually increased over distance, i.e., repeated NEDC driving cycles with different initializations. These observations can be further interpreted in terms of a monetary value by analyzing the costs of driving by the two game-theoretic strategies. This driving cost C, which is resulted from the costs of the power of the engine-generator C_g, battery C_b, and UC pack C_c, is defined by (43) after considering that p_o and p_e are the prices of the oil and electricity for generating one joule energy.

$$C = C_g + C_b + C_c = \sum_{i=1}^{T} \left[p_o P_g(i) + p_e(P_b(i) + P_c(i)) \right]. \quad (43)$$

Consequently, the difference in costs (ΔC) between the two game-theoretic strategies, which indicates the saved money that is made by GP-VP over GP-NVP, is illustrated in Fig 14. It is clear that GT-VP strategy results in lower driving cost comparing with GT-NVP.

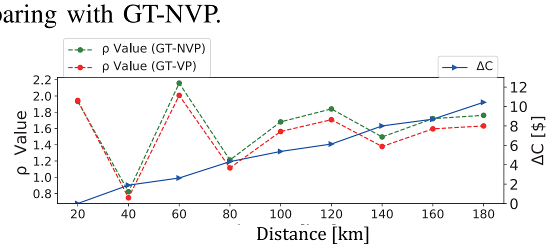

Fig. 14. The overall performance and difference in costs of the two game-theoretic strategies under long-distance driving profile.

Given the above discussions, it can be concluded that the proposed game-theoretic strategy with velocity prediction GT-VP is more effective than the game-theoretic strategy without velocity prediction GT-NVP in short and long-distance driving.

VI. Experiment

To validate the implementable operations of the proposed strategy GT-VP and comparison with GT-NVP, a testbed was set up. The power level of this testbed was downscaled to 60 W to match the capacity of the experimental components. The testbed in experiment was configured to be similar in practice to that of the vehicle's powertrain, i.e., the system configuration in Fig. 1. In this testbed, the power supply emulates the role of the engine-generator along with its AC/DC converter. Whereas, the electronic load acts as the load demand of the vehicle. The battery pack and the UC pack as well as its DC/DC converter are implemented by real devices. The sampling resistors are used for current measurements. The CompactRIO controller controls the power-width-modulation of the DC/DC converter and the host PC is used for observing the results. The specifications of these components are summarized in Table III and the block diagram connections among them are illustrated in Fig. 15(b). Here, the solid lines indicate the power connections whereas the dotted lines indicate the signal communications.

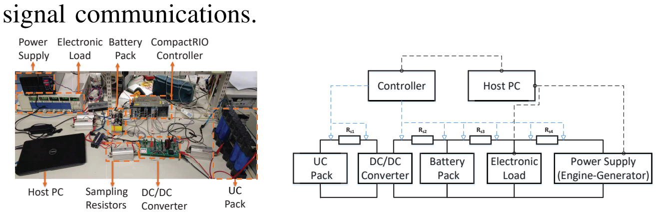

(a) (b)

Fig. 15. The experimental setup of the onboard HESS (a) Downscaled testbed. (b) Block diagram.

TABLE III
Specifications for Major Components

Power Supply (Takasago ZX-800L)	Max power: 800 W (0-80V, 0-80A)
Electronic Load (1 Kikusui PLZ-50F/150U)	Max power: 600 W (1 PLZ-50F, 4 PLZ150USs with 1.5-150 V, 0-30 A each)
DC-DC Converter (Design/fabricated in house)	Max power: 100 W Switch Frequency: 20 kHz
Li-ion Battery Pack (BESS) (Lishen LP2770102AC)	Four cells (series), 12.5 Ah/cell, 3.2 V/cell (nominal voltage)
UC Pack (Nippon Chemi-Con)	Four cells (series), 1760 F/cell, 2.5 V/cell (Max Vol.)
High-accuracy Sampling Resistors (PCN Corporation RH series)	RH250M4 0.01 Ω (± 0.02%)
Control and DAQ System (NI CompactRIO)	I/O board: NI 9401 A/D boards: NI 92192, NI 9203

The two energy management strategies were implemented by Labview platform and the results are shown in Fig. 16 and Table IV. As seen, the experiment results match those in simulation and lead to the same conslusions. Therefore, the proposed GT-VP is not only supreme over GT-NVP in simulation analysis but also in practical implementations.

TABLE IV
Comparison of Evaluation Criteria in Experiment

Driving Cycle	Index	Evaluation Criterion			
		$\mu_{Eg}(w)$	$\mu_{pb}(w)$	$\sigma_{pb}(w^2)$	μ_{Ec}(J)
NEDC	GT-NVP	7432	-0.096	20.13	185632
	GT-VP	7427	-0.299	19.58	182701
	Percentage	-0.067%	2.11	-2.73%	-1.57%

VII. Conclusion

A game-theoretic strategy with velocity prediction was proposed to dispatch the power among the three energy sources

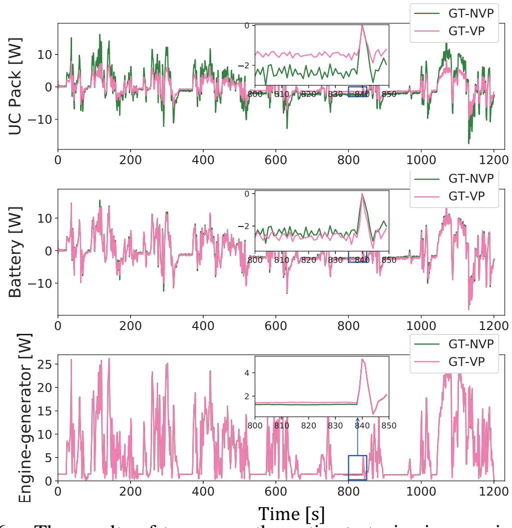

Fig. 16. The results of two game-theoretic strategies in experiment.

of engine-generator, battery, and UC pack in the onboard HESS. The game-theoretic strategy was designed as a non-cooperative game on the basis of the individual preferences of the energy sources. The velocity prediction of the vehicle was implemented by an LSTM network. The training of this neural network was applied by extending the original dataset with utilizing feature extraction. A multiple time-series method is newly applied to group the input features according to the target prediction horizon. Moreover, the predicted information is added into the utility functions of these three energy sources in the non-cooperative game. The solution, i.e., Nash Equilibrium, of the proposed GT-VP was reached through the best response functions of the energy sources. The comparisons of the two game-theoretic strategies in both short-distance and long-distance driving scenarios were analyzed in simulation. Comparing with the GT-NVP, the proposed GT-VP showed better performance both in short-distance and long-distance driving scenarios in simulation. The results in simulation and experiment demonstrated that the GT-VP is superior than the GT-NVP by reducing fossil fuels, prolonging battery life and lowering the driving cost. Moreover, the robustness and sensitivity of the proposed strategy were validated through case studies with increasing velocity prediction error. Even though, there are still some limitations of the proposed GT-VP strategy. For example, the velocity prediction costs the expense of computational burden. The proposed strategy can't work properly if the prediction error is too large. Therefore, the future work for this paper could be further improve the prediction process by including more realistic information such as traffic and weather conditions.

References

[1] C. M. Martinez, X. Hu, D. Cao, E. Velenis, B. Gao, and M. Wellers, "Energy management in plug-in hybrid electric vehicles: Recent progress and a connected vehicles perspective," *IEEE Trans. Veh. Technol*, vol. 66, no. 6, pp. 4534–4549, 2017.

[2] A. Demircalı, P. Sergeant, S. Koroglu, S. Kesler, E. Öztürk, and M. Tumbek, "Influence of the temperature on energy management in battery-ultracapacitor electric vehicles," *J. Cleaner Prod.*, vol. 176, pp. 716–725, 2018.

[3] K. Sarrafan, D. Sutanto, K. M. Muttaqi, and G. Town, "Accurate range estimation for an electric vehicle including changing environmental conditions and traction system efficiency," *IET Electr. Syst. Transp.*, vol. 7, no. 2, pp. 117–124, 2016.

[4] X. Hu, C. M. Martinez, and Y. Yang, "Charging, power management, and battery degradation mitigation in plug-in hybrid electric vehicles: A unified cost-optimal approach," *Mech. Syst. Sig. Process.*, vol. 87, pp. 4–16, 2017.

[5] F. Akar, Y. Tavlasoglu, and B. Vural, "An energy management strategy for a concept battery/ultracapacitor electric vehicle with improved battery life," *IEEE Trans. Transport. Electrific.*, vol. 3, no. 1, pp. 191–200, 2017.

[6] M. A. Mohamed, T. Jin, and W. Su, "Multi-agent energy management of smart islands using primal-dual method of multipliers," *Energy*, vol. 208, no. C, 2020. [Online]. Available: https://ideas.repec.org/a/eee/energy/v208y2020ics0360544220314134.html

[7] H. Yin, C. Zhao, M. Li, C. Ma, and M.-Y. Chow, "A game theory approach to energy management of an engine-generator/battery/ultracapacitor hybrid energy system." *IEEE Trans. Ind. Electron.*, vol. 63, no. 7, pp. 4266–4277, 2016.

[8] H. Yin, C. Zhao, and C. Ma, "Decentralized real-time energy management for a reconfigurable multiple-source energy system," *IEEE Trans. Ind. Informat.*, vol. 14, no. 9, pp. 4128–4137, 2018.

[9] T. Lan, K. Jermsittiparsert, S. T. Alrashood, M. Rezaei, L. Al-Ghussain, and M. A. Mohamed, "An Advanced Machine Learning Based Energy Management of Renewable Microgrids Considering Hybrid Electric Vehicles Charging Demand," *Energies*, vol. 14, no. 3, pp. 1–25, January 2021. [Online]. Available: https://ideas.repec.org/a/gam/jeners/v14y2021i3p569-d485529.html

[10] P. Wang, D. Wang, C. Zhu, Y. Yang, H. M. Abdullah, and M. A. Mohamed, "Stochastic management of hybrid ac/dc microgrids considering electric vehicles charging demands," *Energy Reports*, vol. 6, pp. 1338–1352, 2020. [Online]. Available: https://www.sciencedirect.com/science/article/pii/S235248472030593X

[11] J. Xu, A. Alsabbagh, D. Yan, and C. Ma, "Game-theoretic energy management with velocity prediction in hybrid electric vehicle," in *2019 IEEE 28th International Symposium on Industrial Electronics (ISIE)*, 2019, pp. 1084–1089.

[12] C. Sun, "Velocity predictors for predictive energy management in hybrid electric vehicles." *IEEE Trans. Contr. Sys. Techn.*, vol. 23, no. 3, pp. 1197–1204, 2015.

[13] Z. Cheng, M. Chow, D. Jung, and J. Jeon, "A big data based deep learning approach for vehicle speed prediction," in *Int. Symp. Ind. Electron.*, 2017, pp. 389–394.

[14] B. Jiang and Y. Fei, "Vehicle speed prediction by two-level data driven models in vehicular networks," *IEEE Trans. Intell. Transp. Syst.*, vol. 18, no. 7, pp. 1793–1801, 2017.

[15] K. Vatanparvar, S. Faezi, I. Burago, M. Levorato, and M. A. Al Faruque, "Extended range electric vehicle with driving behavior estimation in energy management," *IEEE Trans. Smart Grid*, vol. 10, no. 3, pp. 2959–2968, 2019.

[16] A. Khalid and A. I. Sarwat, "Unified univariate-neural network models for lithium-ion battery state-of-charge forecasting using minimized akaike information criterion algorithm," *IEEE Access*, vol. 9, pp. 39 154–39 170, 2021.

[17] A. Khalid, A. Sundararajan, I. Acharya, and A. I. Sarwat, "Prediction of li-ion battery state of charge using multilayer perceptron and long short-term memory models," in *2019 IEEE Transportation Electrification Conference and Expo (ITEC)*, 2019.

[18] X. Hao, Q. H. Du, and M. Reynolds, "A location-velocity-temporal attention lstm model for pedestrian trajectory prediction," *IEEE Access*, vol. PP, no. 99, pp. 1–1, 2020.

[19] J. Shin, K. Yeon, S. Kim, M. Sunwoo, and M. Han, "Comparative study of markov chain with recurrent neural network for short term velocity prediction implemented on an embedded system," *IEEE Access*, vol. 9, pp. 24 755–24 767, 2021.

[20] A. Kuperman and I. Aharon, "Battery–ultracapacitor hybrids for pulsed current loads: A review," *Renew. Sust. Energ. Rev.*, vol. 15, no. 2, pp. 981–992, 2011.

[21] H. Rahimi-Eichi and M. Chow, "Big-data framework for electric vehicle range estimation," in *IEEE Annu. Conf. Ind. Electron. Soc.*, 2014, pp. 5628–5634.

[22] C. Sun, X. Hu, S. J. Moura, and F. Sun, "Velocity predictors for predictive energy management in hybrid electric vehicles," *IEEE Trans. Control Syst. Technol.*, vol. 23, no. 3, pp. 1197–1204, 2014.

[23] J. Shen, S. Dusmez, and A. Khaligh, "Optimization of sizing and battery cycle life in battery/ultracapacitor hybrid energy storage systems for electric vehicle applications," *IEEE Trans. Ind. Informat.*, vol. 10, no. 4, pp. 2112–2121, 2014.

Juanting Xu received the B.S. degree in automation from Nanjing University, Nanjing, China, in 2017, and the M.S. degree of science in control science and engineering from the University of Michigan-Shanghai Jiao Tong University Joint Institute, Shanghai Jiao Tong University, Shanghai, China, in 2020. Her research interests include game theory, time-series forecasting, multi-agent modeling, and applications in distributed systems such as hybrid energy system and micro/smart grids.

Miss Xu served as a technical paper reviewer in IEEE Transactions on Industrial Informatics and the 44th Annual Conference of the IEEE Industrial Electronics Society in 2018. She served as a Session Chair at The 28^{th} IEEE International Symposium on Industrial Electronics, June 12-14, 2019, Vancouver, BC, Canada. She won the IEEE-IES student paper travel assistance award in 2019 and was awarded as outstanding graduate of Shanghai Jiao Tong University in 2020.

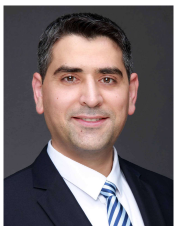

Amro Alsabbagh (S'16-M'20) received the B.S. and M.S. degrees both in the automatic control and computers engineering from Al-Baath University, Homs, Syria, in 2010 and 2015, respectively, and the Ph.D. degree in control science and engineering from the University of Michigan-Shanghai Jiao Tong University Joint Institute, Shanghai Jiao Tong University, Shanghai, China, in 2020. Currently, he is a postdoctoral fellow at polytechnique Montreal, Quebec, Canada. His research interests include modeling and control of micro/smart grid.

Dr. Alsabbagh serves as technical paper reviewer in many journals including IEEE Transactions on Industrial Informatics and IEEE Transactions on Industrial Electronics. He served as a session Chair in the 4^{th} IEEE International Conference on Industrial Cyber-Physical Systems, May 10-13, 2021, Victoria, BC, Canada and the 9^{th} IEEE International Power Electronics and Motion Control Conference, Nov. 29-Dec. 2, 2020, Nanjing city, Jiangsu, China. He won the IEEE-IES student paper travel assistance award in 2018 and the Shanghai Jiao Tong University Excellent International Post-Graduate Students in 2020.

Chengbin Ma (M'05-SM'18) received the B.S. degree in industrial automation from East China University of Science and Technology, Shanghai, China, in 1997, and the M.S. and Ph.D. degrees in electrical engineering from The University of Tokyo, Tokyo, Japan, in 2001 and 2004, respectively. From 2004 to 2006, he was an R&D Researcher with the Servo Motor Laboratory, FANUC Limited, Japan. Between 2006 and 2008, he was a Postdoctoral Researcher with the Department of Mechanical and Aeronautical Engineering, University of California, Davis, USA. He joined the University of Michigan-Shanghai Jiao Tong University Joint Institute, Shanghai Jiao Tong University, Shanghai, China, in 2008, and currently an Associate Professor of electrical and computer engineering. His research interests include energy management, megahertz wireless power transfer, dynamics and motion control, and wide applications in electronic devices, electric vehicles, microgrids, smart grids, etc.

Dr. Ma is an IEEE senior member. He serves as Delegate of Energy Cluster, Chair of Energy Storage Technical Committee and Chair of Shanghai Chapter, IEEE Industrial Electronics Society. He is an Associated Editor for the IEEE Transactions on Industrial Informatics and IEEE Journal of Emerging and Selected Topics in Industrial Electronics. He won many teaching and research awards at Shanghai Jiao Tong University, such as Koguan Top Ten Best Teacher Award in 2017 and Koguan Top Ten Research Group Award in 2014. He also received Research Excellence Award from AirFuel Alliance, USA, in 2019.